Nuclear Instruments and Methods in Physics Research A274 (1989) 494–500
North-Holland, Amsterdam

# NEUTRON DETECTION EFFICIENCY FOR NE213 AND BC501 SCINTILLATORS AT ENERGIES BETWEEN 25 AND 200 MeV

R.C. BYRD and W.C. SAILOR

*Los Alamos National Laboratory, Los Alamos, NM 87545, USA*

Received 6 June 1988

The $^{7}$Li(p, n) reaction at 0° has been used to measure the response of single-element organic scintillators to monoenergetic neutron beams at five energies between 25 and 200 MeV. Zero-degree cross section data were also obtained for the $^{7}$Li(p, n) reaction for neutron energies down to 20 MeV. The scintillator response data agree within ±20% with differential and integral efficiencies calculated using a standard detector simulation program.

## 1. Introduction

To support a study of preequilibrium neutron emission at medium energies [1], cross sections for (p, n) reactions on $^{90}$Zr and $^{208}$Pb nuclei have been measured at the Indiana University Cyclotron Facility (IUCF) for incident proton energies of 80, 120 and 160 MeV. The data set covers neutron emission angles $\theta_{lab}$ from 0 to 144° and neutron energies extending down to about 20 MeV. A major constraint on the accuracy of the data is the calibration of the energy-dependent efficiency of the neutron detectors. Accordingly, measurements were also made of the 0° yield for the $^{7}$Li(p, n)$^{7}$Be (g.s. + 0.43 MeV) reaction. This particular source reaction provides a nearly monoenergetic peak whose cross section has been calibrated to better than 5% over most of this energy range [2]. The present work extends the efficiency calibrations made during the experiment to energies from 25 to 200 MeV. Measurements at 90 and 140 MeV corroborate the earlier ones at 80, 120 and 160 MeV, while additional data at 30, 55 and 200 MeV extend the calibration over all energies of interest, especially those below 80 MeV.

The present experiment, however, provides more than just the integral efficiency measurements needed to normalize the $^{90}$Zr and $^{208}$Pb(p, n) cross section data. The $^{7}$Li(p, n) time-of-flight spectra were analyzed to obtain double-differential cross sections

$$d^2\sigma/(d\Omega\, dE_n)(0°)$$

for neutron energies down to about 20 MeV. Simultaneous storage of the scintillator pulse height spectra also provides measurements of the differential efficiency at five beam energies, and the use of different scintillators allows important consistency checks. These efficiency measurements can be compared to calculations using the Monte Carlo program developed by Kurz [3], Stanton [4], McNaughton et al. [5] and Cecil et al. [6]. Although the integral efficiencies depend mainly on a small number of total cross sections, the differential data are particularly sensitive to assumptions about the complicated $^{12}$C breakup reactions. Unfortunately, few such measurements [7] exist for neutron energies above 30 MeV, where such breakup reactions begin to dominate the detection efficiency.

This paper describes measurements of the differential cross sections $d^2\sigma/(d\Omega\, dE_n)$ for the $^{7}$Li(p, n) reaction at 0° and of the integral and differential efficiencies for NE213 and BC501 scintillators. Included are comparisons between the efficiency data and calculations made using the code of Cecil et al. Subsequent articles [8,9] will discuss these comparisons in detail and describe similar measurements of the integral efficiency for BC418 scintillator over the same energy range.

## 2. Experimental technique

The measurements reported here used the IUCF (p, n) beam swinger with the cyclotron operating in "stripper-loop" injection mode [10], which provided beam currents of 25–100 nA on target in subnanosecond pulses with separations of 2–3 μs. The $^{7}$Li targets were self-supporting rolled foils with thicknesses from 50 to 212 mg/cm$^2$; the corresponding energy losses were 0.33–3.3 MeV. A collimated $\Delta E$–$E$ telescope was placed at a 10° scattering angle about 150 cm downstream from the target to detect scattered protons. This detector was used during data acquisition to monitor the time structure of the beam; during data analysis it was used to correct the integrated charge for bunching inefficiencies. The unscattered proton beam was swept into a Faraday cup by a beam-dump magnet; any

0168-9002/89/$03.50 © Elsevier Science Publishers B.V.
(North-Holland Physics Publishing Division)

protons scattered into the 0° neutron beam were removed by an additional dipole magnet, supplemented by copper degrader plates inserted at the higher energies. Spectra were obtained with and without the plates to confirm the absence of protons and check the neutron attenuation calculations.

Measurements were made using two different detectors placed near 0° at a distance of 43.5 m from the target. One of the detectors, referred to as the "BC501" detector, was from the set used in the above $^{90}$Zr and $^{208}$Pb(p, n) cross section measurements. It consisted of a cylinder 20.3 cm deep and 30.5 cm in diameter, filled with BC501 scintillator to leave an expansion void 2.5% of the scintillator's volume. The scintillator was optically coupled to a 12.7 cm diameter RCA4522 photomultiplier tube through a conical light guide 9.9 cm long and 11.0 cm in final diameter. The other detector (the "NE213" detector) was a bubble-free cylinder 12.1 cm in a diameter and 12.7 cm deep, filled with NE213 scintillator and coupled to a 5.0 cm photomultiplier tube through a conical light guide. The specified density and hydrogen/carbon ratio for the NE213 scintillator are 0.874 and 1.213; for BC501 the corresponding values [11] are 0.901 and 1.287.

The surfaces of both scintillators were painted with diffuse white reflecting paint. Monte Carlo calculations [8,11] of the photon transport through the scintillators and light guides were made to study the fraction of the light which reached the photomultiplier from different locations throughout the scintillator volume. The results were particularly sensitive to the light attenuation length, for which reported values [12,13] range from 58 to 150 cm, depending on the particular measurement technique. Using a value of 100 cm gives transmission distributions with mean values of 0.089–0.097 and widths of about 0.027 (FWHM), giving pulse height resolutions of about 30% for uniformly illuminated scintillators. As discussed in ref. [8], when combined with the position dependence of the light production, such variations have a profound effect on the detector's pulse height resolution.

The anode signals from the photomultiplier bases were sent some 200 m through low-loss cable to acquisition electronics based on constant-fraction timing discriminators, multi-input TDCs, and charge-integrating ADCs. Both pulse height and time-of-flight data were stored in event mode on magnetic tape for subsequent off-line analysis. An additional event stream was triggered by the timing signal from the scattered-proton monitor. The time-zero marker for both the neutron and proton time-of-flight data was generated from a cyclotron rf signal which was phase-locked to a fast beam pickoff and gated by the stripper-loop extraction trigger.

Both NE213 and BC501 organic scintillators have the capability of discriminating between events due to recoil electrons, protons, deuterons, and alphas. Although this property can be useful in analyzing the relative importance of different detection reactions, at higher energies it complicates the measurement of detection efficiency, since the characteristic ionization differences exist only for those particles which stop within the scintillator volume. As a result, recoil protons which escape the scintillator can be misidentified as electrons, an effect which complicates the analysis of the data and will be discussed in connection with the $^{90}$Zr and $^{208}$Pb cross section measurements.

## 3. Data reduction

The accuracy of the data reported here is determined largely by two factors: normalization of the incident neutron flux and calibration of the pulse-height spectra in terms of standard units of light output. The final error budget for the determination of the absolute flux from the calibrated $^{7}$Li(p, n)$^{7}$Be (0.0 + 0.43 MeV) reaction is given in table 1.

The dominant uncertainty is associated with the calibration of the $^{7}$Li(p, n) cross section. From 80 to 200 MeV the value has been determined to be 37 mb/sr(LAB) with a 3–5% uncertainty [2,14]. The values for 55 and 30 MeV were estimated from the data shown in ref. [14] to be 35 and 28 mb/sr, with 10% and 18% uncertainties, respectively. The mean angles for the detectors were actually 0.5° for the NE213 detector and 1.0° for the BC501 detector; at these angles the cross section differs by much less than 1% from the calibrated zero-degree value [14].

The $^{7}$Li targets were self-supporting foils; the estimated thickness uncertainty was 1.6%. The measurements at 30 and 55 MeV used several different targets to check for foil non-uniformity and beam integration losses due to Coulomb scattering; the maximum variation in yield was 2% between the 50 and 212 mg/cm$^2$ targets used at 30 MeV. The data chosen for presentation below were obtained using the thinnest targets available; the energy losses were usually less than 1 MeV. Although additional charge integration errors can

Table 1
Uncertainties in absolute neutron flux

| Energy [MeV] | 30 | 55 | 90–200 | All |
|---|---|---|---|---|
| Cross section | 18% | 10% | 5% | |
| Target thickness | | | | 1.6% |
| Detector volume | | | | 6% |
| Flight path | | | | 1% |
| Attenuation | | | | 2% |
| Charge integration | | | | <1% |
| Total | 19% | 12% | 8% | |

result from incomplete beam bunching, these errors were reduced to $< 1\%$ by using the proton monitor as discussed in section 4.

A significant factor in calculating the solid angle for the incident flux is estimating the active volume of the liquid scintillators. The uncertainty in the scintillator dimensions and in the size and shape of the air bubble result in an uncertainty of about 6%. An additional 1% uncertainty in the detector solid angle results from a flight path uncertainty of 25 cm.

At long flight paths large corrections must be made for neutron attenuation in air; values ranged from 7% at 200 MeV to 38% at 10 MeV. At 90, 140 and 200 MeV the use of copper degrader plates with thicknesses between 1.3 and 4.5 cm resulted in additional attenuation corrections of 11–32%. Various other materials in the flight path led to further corrections of 10–20%. All attenuations were calculated using parameterizations [15] of the total cross sections which introduced negligible error above 10 MeV; the major uncertainty concerns the composition and amounts of the materials involved. In the case of the copper plates the attenuation was measured by obtaining spectra both with and without the plates; the results agreed with the calculated values to within 1%. The effects of the air and other materials cannot be checked by measurement; the total uncertainty in the combined attenuation corrections was assumed to contribute 2% to the uncertainty in the incident neutron flux.

Even with the stripper loop providing proton beam currents on target of 100 nA at a 2 μs repetition rate, the average neutron detection rate was still below 1 in 1000 beam pulses. The ~150 μs CAMAC conversion times were therefore the major cause of dead times, which ranged from 2% to 30% and were measured with negligible error. The accuracy of these corrections is best demonstrated by the 1% agreement between the measured and calculated copper attenuation values, despite dead time corrections of up to 50% due to the high proton counting rates when the plates were removed. Further confirmation is provided by the agreement of better than 2% between cross sections measured using targets which differed by more than a factor of 4 in thickness.

The second major class of calibrations determines the shape of the detector response in terms of the slope and intercept of the pulse–height scale in units of $MeV_{ee}$. The zero offset and noise level for the complete system of detectors and electronics was measured by triggering the electronics with a random pulser instead of the detector logic output, thus producing an ADC integration over the baseline exactly as for the detector signal. The gain calibration across threshold was determined by measuring the Compton electron spectra for $^{22}Na$ (1.06 $MeV_{ee}$) and $^{228}Th$ (2.39 $MeV_{ee}$) gamma ray sources. The location of the channel corresponding to the Compton edge was determined with corrections for detector resolution [16]. Variable attenuators were then inserted during data acquisition to reduce the 0–160 $MeV_{ee}$ scale expected for 200 MeV protons to the calibrated pulse height scale. The exact attenuator values were measured by comparing spectra obtained at different settings. The calibrated electronic thresholds were $0.25 \pm 0.10$ $MeV_{ee}$ for the NE213 detector and $3.7 \pm 0.2$ $MeV_{ee}$ for the BC501 detector.

Establishing pulse height linearity over a range of 160 $MeV_{ee}$ can be difficult when using anode signals and integrating ADCs. In addition to the possible saturation of the anode signal, there is also the possibility of changes in the pulse shape versus amplitude. These problems were aggravated in the present experiment because high photomultiplier gains and narrow (~100 ns) ADC integration gates were required to reduce the effect of ac line noise introduced over the signal path between the detectors and the acquisition system. To determine gain calibration curves for the two detectors, at each proton energy ratios were obtained between the maximum pulse heights observed in the data and those calculated using the code of Cecil et al. and standard light-output curves [6]. Over the full pulse height range the gain was found to decrease by a factor of 2 for the BC501 detector and by a factor of 4 for the NE213 detector. The only known problems remaining after correcting for this nonlinearity are an uncertainty in the pulse height scale between 3 and 20 $MeV_{ee}$ and a distortion of the normal relationship between resolution and pulse height.

## 4. Presentation of results

Fig. 1 shows the double-differential cross section $d^2\sigma/(d\Omega\, dE_n)(0°)$ (LAB) for the $^7Li(p, n)$ reaction. At each bombarding energy the maximum excitation energy available in $^7Be$ is indicated to the left of the data. The spectra have been normalized so that the integral over the peak at $(0.0 + 0.43)$ MeV gives the calibrated value for the cross section. Near the ground state the cross section values therefore have the absolute uncertainties of 8–19% given in table 1. At other neutron energies the data were obtained by correcting the yields for the calculated energy dependences of the neutron attenuation [15] and detection efficiency [6], resulting in an additional uncertainty which reaches about $\pm 10\%$ near $E_n = 15$ MeV. The present data agree with those of ref. [9] to within $\pm 5\%$ except at $E_p = 55$ MeV, where differences in the energy dependences of the efficiencies result in a discrepancy of about 15%. Other errors can result from neutron scattering from the collimation around the target; shadow-bar measurements made during the $^{90}Zr$ and $^{208}Pb$ measurements indicate that this

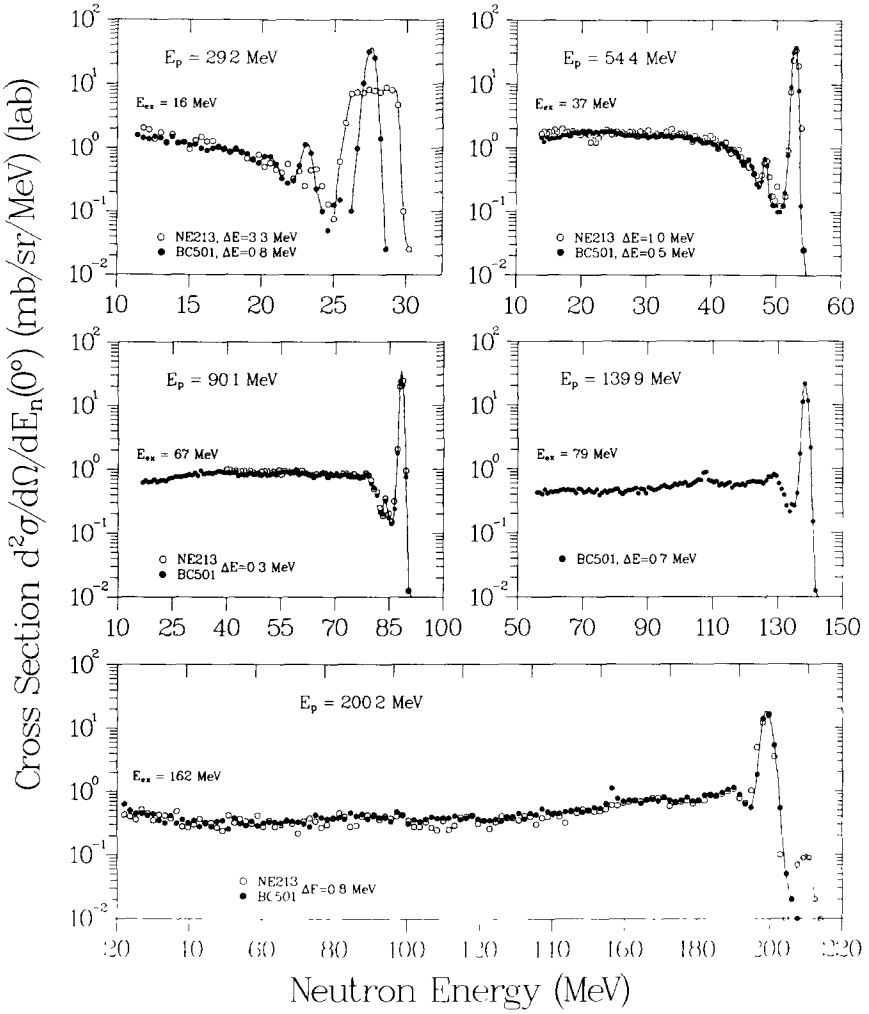


Fig. 1. Differential cross sections $d^2\sigma/(d\Omega\, dE_n)(0°)$(LAB) for the $^7$Li(p, n) reaction. The data have been normalized so that the integral over the ground state peak gives the calibrated 0° value. The bin sizes for the data are 0.4 MeV at 30 and 55 MeV, 0.8 MeV at 90 and 140 MeV, and 1.6 MeV at 200 MeV.

background could have increased the cross section values above 20 MeV by about 5–10%.

Transitions to some of the low-lying states in $^7$Be are seen in fig. 1 at proton energies below 100 MeV. In no case was the $J^\pi = 1/2^-$ state at 0.43 MeV resolved; its yield was always included with that for the $3/2^-$ ground state. At $E_p = 30$ MeV the difference between the shapes of the ground state peaks is due to the large difference in target thicknesses. At $E_p = 29$, 54 and 90 MeV, the $7/2^-$ state at 4.57 MeV has 0° cross sections of $0.8 \pm 0.1$, $0.55 \pm 0.06$, and $0.33 \pm 0.15$ mb/sr, respectively. The unresolved $5/2^-$ states at 6.7 and 7.2 MeV have combined cross sections of about $0.23 \pm 0.1$ and $0.15 \pm 0.05$ mb/sr at the two lowest energies.

A common problem with time-of-flight measurements is the ambiguity in the time-to-energy conversion caused by the simultaneous arrival at the detector of neutrons of different energies from successive beam bursts ("frame overlap"). The stripper loop eliminates this difficulty because the pulse spacings of 2–3 μs are large enough to avoid any ambiguity for neutron energies down to well below 10 MeV. However, another problem can result from instabilities in the phasing between the stripper loop, the injection bunching, and the cyclotron, causing the acceleration of small amounts of beam in cyclotron pulses adjacent to the primary pulse. The result is a time-shifted image of the main spectrum, usually offset by one cyclotron period (28–37 ns) from the main pulse. The peak shown in the 200 MeV spectrum for the NE213 detector near $E_n = 210$ MeV is such an image, as is that for the BC501 detector in the 200 MeV spectrum near $E_n = 160$ MeV and in the 140 MeV spectrum near $E_n = 110$ MeV. Such image problems were minimized by using the time spectrum

from the proton monitor, which records the time distribution of the beam throughout the period between stripper loop pulses. During data acquisition this information was used to adjust the buncher phasing; during data analysis it was used to correct the integrated charge for the fraction of the beam not located in the primary pulse. The worst case was the 6% correction applied to BC501 spectrum at $E_p = 200$ MeV.

A final correction was introduced for cosmic ray events, which contribute a constant background to the time-of-flight spectra. Because the time-to-energy transformation $dt/dE_n$ is proportional to $1/(\beta\gamma)^3$, the effect of this contribution increases rapidly for lower energies. At the flight path used here, the compression in the time-to-energy conversion increases by a factor of 100 as the neutron energy decreases from 200 to 10 MeV. At $E_d = 30$ MeV the backgrounds which were subtracted were as large as 0.20 mb/(sr MeV) for the BC501 detector and 0.05 mb/(sr MeV) for the NE213 detector – a ratio proportional to the horizontal projection of the detector areas. In all other cases no correction was applied, since the maximum contribution was much less than 10% of the cross section. Again, the small size of this correction is due largely to our use of the stripper loop, which in effect increases the beam intensity on target by a factor of 10.

Pulse height spectra for five incident neutron energies were obtained by selecting events in the ground state peak at each proton energy. These spectra are shown in fig. 2 along with corresponding calculations using the program of Cecil et al. [6]. All spectra have been normalized to an incident flux of $10^6$ neutrons and divided by the scintillator thickness in gm/cm$^2$ to allow both detectors to be compared on the same scale.

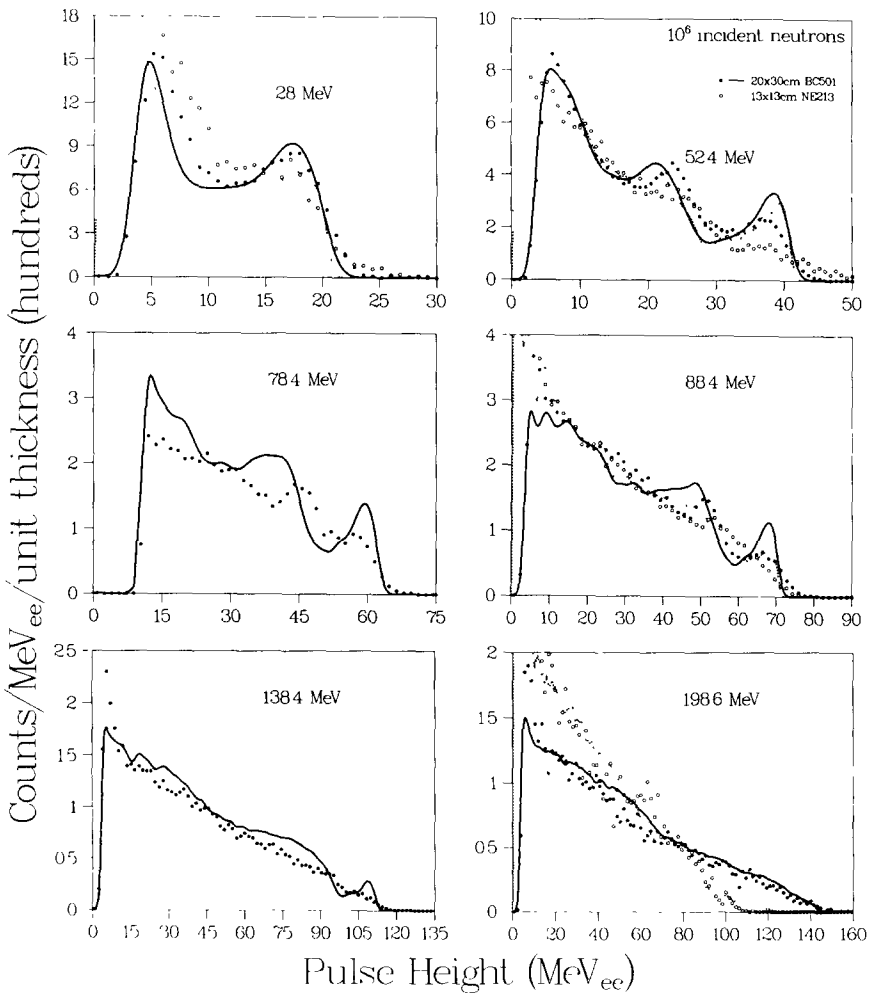


Fig. 2. Differential efficiencies for NE213 and BC501 scintillators, normalized to the scintillator thickness in g/cm$^2$. The data are from the present experiment, and the calculations were made using the code of Cecil et al. [6]. As discussed in section 4, the BC501 data have been renormalized by 1.14, the NE213 data by 0.83.

To simplify comparison of the shapes, the data have been renormalized as discussed below, with the BC501 data increased by 1.14, the NE213 data reduced by 0.83.

Significantly, the renormalization for the BC501 spectra also applies to data obtained during two separate $^{90}$Zr and $^{208}$Pb(p, n) cross section measurements [1,17] at 80 and 160 MeV, as represented by the 80 MeV spectrum included here. The detectors used at 80 and 160 MeV were different ones from a set of five, but were interchangeable in all respects with the particular one used for the present data. The original pulse height scale for this spectrum was determined from gamma ray calibrations; it was renormalized by 1.16 to match the calculated recoil edge. Because the electronics used for this spectrum was based on slow pulse-shaping amplifiers and peak detecting ADCs, the pulse height resolution and linearity should be better than those for the present data.

The comparison between measurements and calculations will be discussed in detail in a forthcoming article [8], so only a few comments will be made here. First, a prominent feature of both the data and the calculations is the dramatic energy variation of the recoil edges associated with n–p scattering and $^{12}$C breakup, all of which disappear as the maximum proton range approaches the size of the scintillator. Second, in both detectors the resolution in the calculations is much better than that observed in the measurements, especially at higher pulse heights. This discrepancy is due mainly to two instrumental effects which were not included in the calculations. Most important is the ~ 20–30% resolution broadening associated with the non-uniform light collection. In addition, for the NE213 data in particular the compression of the raw spectra at the higher pulse heights makes the contribution of ac line noise greater than the constant value included in the resolution function. Calculations which estimate these effects produce spectra whose shapes are much more like those of the data. More definitive results are obtained by the calculations of ref. [8], which correctly account for the position correlations between light production and transmission.

The reason for the renormalization shown in fig. 2 is apparent in fig. 3, which shows the integrated efficiencies for a 6 MeV$_{ee}$ threshold, again divided by the detector thickness in g/cm$^2$. In the case of the calculations, the efficiency per unit thickness is essentially the same for the two detectors. The calculated neutron detection rate is therefore proportional to the detector mass, indicating that edge effects and self-attenuation cause little efficiency loss at these energies for scintillators of 10–20 cm thickness. The calculated efficiency is also insensitive to resolution effects such as noise contributions, non-uniform light collection, and pulse height nonlinearity, since at 6 MeV$_{ee}$ the distribution is relatively flat and few counts can be shifted across threshold.

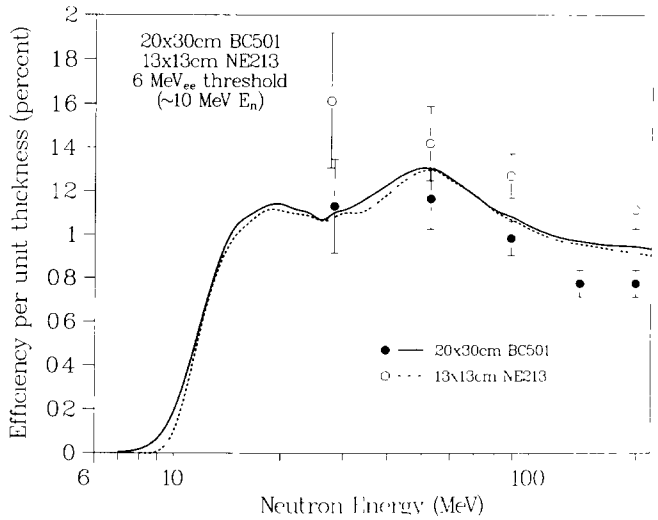


Fig. 3. Comparison between measured and calculated integral efficiencies for NE213 and BC501 scintillators, normalized to the scintillator thickness in g/cm$^2$. The data are from the present experiments, and the calculations were made using the code of Cecil et al. [6].

Calculations of these effects produced less than a 1% change in the integral efficiency. Similarly, for low thresholds changes in the light output coefficients have little effect. Changing the proton and alpha particle functions from those of ref. [6] to those of ref. [18] caused a 1.4% change in the efficiency at 28 MeV and less than a 0.5% change at the other energies. In short, the calculated efficiencies per unit thickness for the two detectors are the same to within 2% at all energies.

In the case of the data, the accuracy is best discussed by separating effects due to the flux and shape calibrations. For the shape uncertainties, even with the corrections for nonlinearity the uncertainty in the 6 MeV$_{ee}$ threshold is only about 1.5 MeV$_{ee}$, which increases the uncertainty in the efficiency by 7.7% at 30 MeV and 4.3% at 200 MeV. These uncertainties are supported by the agreement shown in fig. 2 between the calculations and the renormalized data. For the flux determination most of the factors in table 1 cancel in a comparison between the two detectors, leaving only about a 7% uncertainty which is due mostly to the volume uncertainties. The total uncertainty in the ratio of the measured efficiencies is therefore about 8–11%. The difference of about 30% between the BC501 and NE213 measurements is then three times larger than the expected value.

Finally, additional confirmation for the present data is provided by related measurements. First, the present data were measured at IUCF at the same time as those reported in ref. [9] for a small BC418 scintillator. The BC418 efficiencies measured at IUCF agree with earlier measurements for the same detector made at Los Alamos

National Laboratory (LANL). This agreement in turn supports the normalization of the present measurements, since the fluxes incident on the three detectors differ mainly by their solid angles. Second, the present BC501 efficiency measurements agree with earlier ones at 80 and 160 MeV obtained during the $^{90}$Zr and $^{208}$Pb(p, n) cross section experiments. Nevertheless, all three sets of BC501 efficiencies are about 10–20% lower than the values calculated using the code of Cecil et al., while for the BC418 detector the measurements at both IUCF and LANL are in fair agreement with the corresponding calculations.

## 5. Conclusions

The differential efficiencies presented in this work provide a basis for developing calculations of the response of scintillators to medium energy neutrons. As discussed in ref. [8], the effects of different assumptions about the reactions, kinematics and cross sections in the calculations can be tested by comparison to various structures in the data. Although the shapes of the measured distributions agreed well with those calculated using the standard code of Cecil et al., the magnitudes of the measured efficiencies for the two detectors are inexplicably different from the calculations and from one another. Finally, the clean measurements of the $^{7}$Li(p, n) cross section at very high excitation energies in $^{7}$Be demonstrate the quality of data obtainable using the large pulse separations available with the IUCF stripper loop.

## Acknowledgements

We thank W. Scobel and M. Blann for the loan of BC501 detector used in these measurements. R. Kinser, J. Ryan, C. Foster and K. Komisarcik provided the support necessary to set up the experiment at IUCF, and C. Goulding and M. Meier helped with the data acquisition. The copy of the code written by Cecil et al. was provided by B. Anderson.

## References

[1] M. Blann, B.A. Pohl, W. Scobel, M. Trabandt, S.M. Grimes, R. Byrd and C.C. Foster, IUCF Scientific and Technical Report-1986, Indiana University Cyclotron Facility, Bloomington, IN (1987) 88.
[2] T.N. Taddeucci, LANL, private communication (1988).
[3] R.J. Kurz, UCRL-11339 (1964).
[4] N.R. Stanton, Ohio State University Report COO-1545-92 (1971).
[5] M.W. McNaughton, N.S.P. King, F.P. Brady and J.L. Ullmann, Nucl. Instr. and Meth. 129 (1975) 241.
[6] R.A. Cecil, B.D. Anderson and R. Madey, Nucl. Instr. and Meth. 161 (1979) 439;
see also B.D. Anderson, R.A. Cecil and R. Madey, in: The (p, n) Reaction and the Nucleon–Nucleon Force, eds. C.D. Goodman et al. (Plenum Press, New York, 1980) p. 333.
[7] R.A.J. Riddle, G.H. Harrison, P.G. Roos and M.J. Saltmarsh, Nucl. Instr. and Meth. 121 (1974) 445;
P.T. Debevec, G.L. Moake and P.A. Quin, Nucl. Instr. and Meth. 166 (1979) 467;
Hideyuki Sakai, Nobuyuki Matasuoka, Takane Saito and Atsushi Sakaguchi, Nucl. Instr. and Meth. A247 (1986) 515.
[8] W.C. Sailor, R.C. Byrd and Y. Yariv, LANL report LA-11348-MS (1988).
[9] W.B. Amian, M.M. Meier, R.C. Byrd, C.A. Goulding and C.E. Moss, to be published.
[10] D. Friesel, IUCF Scientific and Technical Report-1986 (see [ref.] 1) 112.
[11] B.A. Pohl, LLNL, private communication (1988).
[12] K. Komisarcik, IUCF, private communication (1988).
[13] R. De Leo, G. d'Erasmo, A. Pantaleo and G. Russo, Nucl. Instr. and Meth. 119 (1974) 559.
[14] T.N. Taddeucci, C.A. Goulding, T.A. Carey, R.C. Byrd, C.D. Goodman, C. Gaarde, J. Larsen, D. Horen, J. Rapaport and E. Sugarbaker, Nucl. Phys. A469 (1987) 125.
[15] T.N. Taddeucci, Computer program ATTENE, private communication (1987).
[16] G. Dietze and H. Klein, Nucl. Instr. and Meth. 193 (1982) 549.
[17] M. Trabandt, University of Hamburg, private communication (1987).
[18] J. Rapaport, Ohio University, private communication (1987).